J Nanostruct 16(1): 860-873, Winter 2026

RESEARCH PAPER

Chemo/Phototherapy of Cancer using Camptothecin Supported on $CuFe_2O_4$ (CPT@$CuFe_2O_4$) for Improvement of Chemo-Dynamic Therapy

Fozilov Uktam [1], Khurshed Kurbonov [2], Zubtiyev Sardor [3], Nigora Madaminova [4], Irina Dmitrieva [5], Yuldashev Jurabek [6], Tuychiyev Sardor [7], Boltayev Mashrabjon [8], Iskandarov Jahongir [8], Shamshod Axmedov [9], Ergashev Xudoynazar [10], Xoliqov Tolibjon [10], Sobirjonov Sohibjon [11]*

[1] *Department of Orthopedist Dentistry va Orthodontics, Bukhara State Medical Institute named after Abu Ali ibn Sino, Bukhara, Republic of Uzbekistan*

[2] *Department of Histology, Cytology and Embryology, Samarkand State Medical University, Samarkand, Republic of Uzbekistan*

[3] *Tashkent State Medical University, Tashkent, Republic of Uzbekistan*

[4] *Department of Otorhinolaryngology, Andijan State Medical Institute, Andijan, Republic of Uzbekistan*

[5] *Tashkent State Technical University, Tashkent, Republic of Uzbekistan*

[6] *Department of Clinical Sciences, Mamun University, Urgench, Republic of Uzbekistan*

[7] *Department of Medicine, Turon University, Karshi, Republic of Uzbekistan*

[8] *Department of Oncology, Bukhara State Medical Institute named after Abu Ali ibn Sino, Bukhara, Republic of Uzbekistan*

[9] *Department of Pharmacology, Bukhara State Medical Institute named after Abu Ali ibn Sino, Bukhara, Republic of Uzbekistan*

[10] *Samarkand Institute of Economics and Service, Samarkand, Republic of Uzbekistan*

[11] *Department of "Medical and bilogical chemistry", Ferghana medical institute of public health, Ferghana, Republic of Uzbekistan*

ARTICLE INFO

Article History:
Received 12 August 2025
Accepted 27 December 2025
Published 01 January 2026

Keywords:
Camptothecin
Chemo-dynamic therapy
Chemotherapy
$CuFe_2O_4$
Phototherapy

ABSTRACT

We report a rationally designed theranostic nanoplatform that integrates chemotherapy, photothermal therapy (PTT), and photo-enhanced chemodynamic therapy (CDT) in a single CPT@$CuFe_2O_4$ nanohybrid. Camptothecin (CPT), a hydrophobic topoisomerase I inhibitor, is non-covalently loaded onto CuFe2O4 spinel nanoparticles, yielding a core–shell–like construct that preserves the CuFe2O4 spinel framework while presenting an amorphous CPT surface layer. Comprehensive characterization (FE-SEM, FT-IR, XRD) confirms preserved crystallinity of the $CuFe_2O_4$ core and successful CPT incorporation without deleterious phase changes or CPT crystallization. The system exploits a triple-action mechanism: (i) CPT provides targeted chemotherapeutic cytotoxicity; (ii) $CuFe_2O_4$ serves as a robust near-infrared (NIR)–absorbing photothermal transducer ($\eta \approx 32.7\%$, ΔT up to ~55 °C at 100 μg/mL); and (iii) the $CuFe_2O_4$ core catalyzes Fenton-like reactions to generate hydroxyl radicals (•OH) from endogenous H_2O_2, with photothermal heating accelerating CDT (photo-enhanced CDT). In vitro experiments in MCF-7 cells reveal strong synergistic cytotoxicity under 808 nm irradiation (Bliss SI values 1.8–2.4), with complete triple-modal eradication observed at clinically relevant CPT/NP concentrations (~100 μg/mL CPT-equivalent, 2 μM CPT). Collectively, CPT@$CuFe_2O_4$ demonstrates a potent, on-demand, multimodal cancer therapy platform that leverages localized photothermal heating to amplify endogenous CDT while delivering CPT at the tumor site. Potential translational relevance is discussed in the context of hypoxia-insensitive CDT and reduced systemic toxicity.

How to cite this article
Uktam F., Kurbonov K., Sardor Z. Chemo/Phototherapy of Cancer using Camptothecin Supported on $CuFe_2O_4$ (CPT@$CuFe_2O_4$) for Improvement of Chemo-Dynamic Therapy. J Nanostruct, 2026; 16(1):860-873. DOI: 10.22052/JNS.2026.01.076

* *Corresponding Author Email: uktam.fozilov@bsmi.uz*

INTRODUCTION

The evolution of cancer therapy has progressively shifted from monomodal interventions towards sophisticated combinatorial strategies designed to overcome resistance and enhance therapeutic specificity [1-3]. Among these, the integration of chemotherapy with phototherapy namely photodynamic (PDT) or photothermal (PTT) therapy has emerged as a particularly compelling paradigm [4-6]. This synergy, often termed chemo/phototherapy, leverages the spatiotemporal precision of light to trigger localized effects that can simultaneously amplify chemotherapeutic efficacy and minimize systemic toxicity [7, 8]. Historically, the field was galvanized by early photodynamic agents like porphyrins, but its scope has dramatically expanded with the advent of advanced nanomaterials. The core principle is multifunctionality: a single agent or platform can deliver a cytotoxic drug while also converting absorbed light into either reactive oxygen species (ROS) for PDT or heat for PTT. This dual-action mechanism not only directly damages tumor cells but can also disrupt tumor vasculature, modulate the immunosuppressive microenvironment, and sensitize cells to the co-delivered chemotherapeutic agent. The strategic importance of chemo/phototherapy lies in its capacity to address the pharmacokinetic mismatch often seen in separate drug and photosensitizer administration, ensuring synchronized action at the target site. Applications now extend beyond oncology into antimicrobial treatments and diagnostics, though its most transformative potential remains in combating solid tumors where external light penetration is feasible. The ongoing challenge, and thus the focus of contemporary research, is the rational design of integrated, stimulus-responsive platforms that optimize the crosstalk between these therapeutic modalities for a concerted and devastating attack on malignant cells.

The strategic application of engineered nanoparticles has been instrumental in transcending the fundamental physicochemical and biological barriers that have long hampered the clinical translation of chemo/phototherapeutic agents [9-12]. For hydrophobic chemotherapeutics like camptothecin (CPT) [13-15], nanoparticles provide an indispensable vector, enhancing aqueous solubility, prolonging systemic circulation,

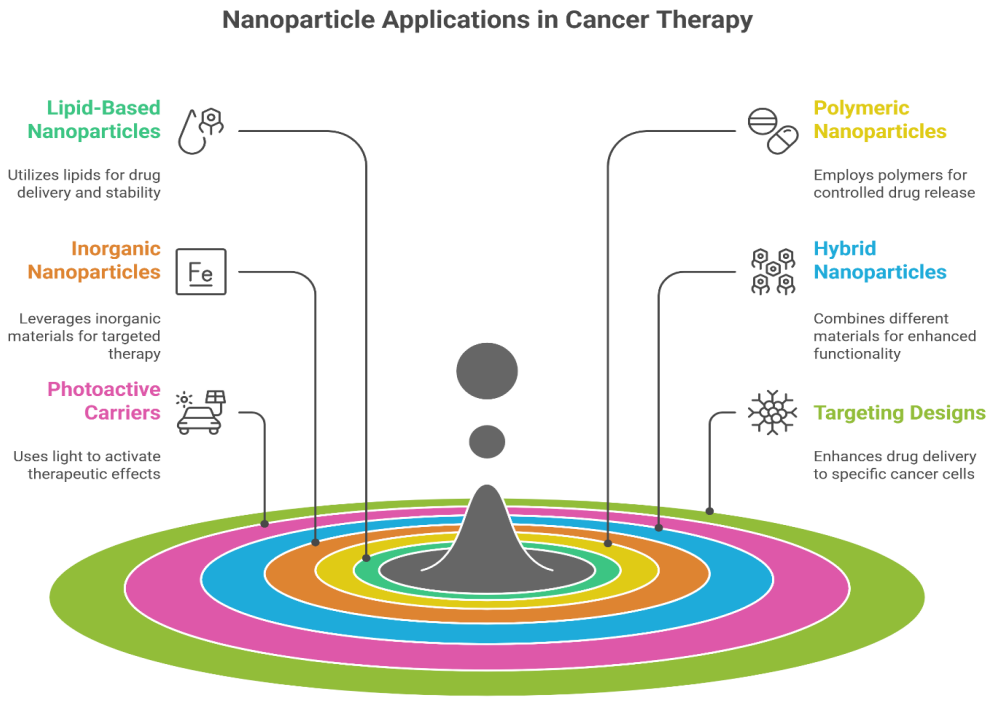

Fig. 1. Different nanoparticle applied in cancer therapy.

and facilitating passive tumor accumulation via the enhanced permeability and retention (EPR) effect [16]. Beyond mere delivery, the nanoparticle core itself can be meticulously designed as a multimodal platform. In the context of phototherapy, nanoparticles composed of semiconductors or plasmonic materials serve as highly efficient energy transducers, converting absorbed near-infrared (NIR) light into local heat for photothermal therapy (PTT) or generating reactive oxygen species (ROS) for photodynamic therapy (PDT) [17-19]. More recently, the integration of Fenton or Fenton-like catalysts, such as transition metal-based spinel ferrites, into these nanostructures has unlocked a powerful combination: photo-enhanced chemodynamic therapy (CDT) [20, 21]. In this paradigm, the photothermal effect can locally increase intratumoral temperature, dramatically accelerating the catalytic conversion of endogenous H_2O_2 into highly cytotoxic •OH radicals. Thus, a single nanostructure can concurrently function as a targeted drug depot, a photothermal agent, and a catalytically active center for CDT, creating a potent and spatially controlled triple-therapeutic synergy against malignant cells.

Recent research into camptothecin (Fig. 2) (CPT)-based chemo/phototherapy platforms reflects a concerted effort to overcome the drug's notorious hydrophobicity and lactone ring instability while amplifying its therapeutic index through synergistic mechanisms. Contemporary strategies have moved beyond simple encapsulation, focusing instead on sophisticated nano-constructs where CPT is either covalently conjugated to polymeric backbones or physically loaded into stimuli-responsive matrices. A prominent trend involves coupling CPT with photothermal agents such as gold nanostructures, polydopamine, or copper sulfide. In these systems, near-infrared (NIR) irradiation not only triggers localized hyperthermia for photothermal therapy (PTT) but also promotes the controlled release of CPT from the nanocarrier, often through thermal decomposition of labile bonds or enhanced diffusion. Furthermore, recent work has demonstrated that the photothermal effect can sensitize cancer cells to chemotherapy by improving drug permeability and inhibiting DNA repair pathways. More advanced designs incorporate additional functionalities; for instance, CPT has been co-delivered with photosensitizers like chlorin e6 in metal-organic frameworks (MOFs) or carbon-based nanoparticles to enable simultaneous PDT and chemotherapy [22-25]. However, a critical gap remains in seamlessly integrating a Fenton-catalytic function to leverage the generated heat for enhancing chemodynamic therapy (CDT) efficacy. While studies employing iron-based nanoparticles (e.g., Fe_3O_4) for combined CPT delivery and CDT exist, the exploration of bifunctional spinel ferrites like $CuFe_2O_4$ which offer superior photothermal conversion and catalytic activity due to mixed valence states as a unified platform for CPT delivery, PTT, and enhanced CDT, represents a compelling and underexplored frontier in the design of multimodal anticancer agents.

Prominent strategies include the encapsulation

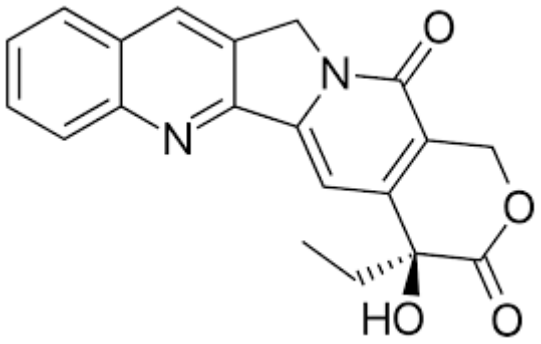

Fig. 2. The chemical structure of camptothecin (CPT).

of CPT within polymeric micelles, liposomes, or mesoporous silica nanoparticles, which are often co-functionalized with photodynamic agents like chlorins or photothermal agents such as indocyanine green or polydopamine. These constructs have demonstrated promising *in vitro* and *in vivo* outcomes, where light irradiation can trigger drug release and simultaneously induce photothermal ablation or ROS generation, yielding a synergistic therapeutic effect. However, these systems are frequently hampered by significant limitations. A primary concern is the premature, non-specific leakage of CPT from the nanocarrier due to weak physical encapsulation, leading to off-target toxicity and reduced tumor accumulation. Furthermore, many designs rely on exogenous, oxygen-dependent photosensitizers, the efficacy of which is severely compromised in the hypoxic tumor microenvironment. Critically, the phototherapeutic and chemotherapeutic components often operate on parallel, rather than interactively amplified, pathways. This represents a missed opportunity; an ideal platform would leverage the photonic energy not only for direct cell killing and drug release but also to catalytically enhance a secondary therapeutic mechanism intrinsically, such as chemodynamic therapy (CDT). Addressing this gap necessitates moving beyond simple co-delivery towards the rational design of a unitary nanoplatform where CPT is strategically coupled with a material whose photoresponse directly potentiates a complementary cytotoxic pathway.

This study aims to design, synthesize, and evaluate a novel nanohybrid in which camptothecin is strategically supported on $CuFe_2O_4$ nanoparticles, thereby integrating chemotherapy, photothermal therapy, and photo-enhanced chemodynamic therapy into a single, synergistic agent for targeted cancer treatment.

MATERIALS AND METHODS

Chemicals and equipment

All chemical reagents were of analytical grade and used without further purification unless otherwise stated. Camptothecin (CPT, >98% HPLC purity) was sourced from Tokyo Chemical Industry (TCI, Japan). Copper(II) nitrate trihydrate ($Cu(NO_3)_2{\cdot}3H_2O$, ≥99%), iron(III) nitrate nonahydrate ($Fe(NO_3)_3{\cdot}9H_2O$, ≥98%), and sodium hydroxide (NaOH, pellets, ≥97%) were procured from Sigma-Aldrich (USA). Ethylene glycol (EG, 99%) and absolute ethanol (C_2H_5OH, 99.9%) were obtained from Merck (Germany). Deionized water (18.2 MΩ·cm resistivity) was produced in-house using a Millipore Milli-Q water purification system. For the photothermal and *in vitro* experiments, phosphate-buffered saline (PBS, pH 7.4) was prepared from tablets supplied by Thermo Fisher Scientific. Dulbecco's Modified Eagle Medium (DMEM), fetal bovine serum (FBS), penicillin-streptomycin, and the Cell Counting Kit-8 (CCK-8) were purchased from Gibco and Dojindo Laboratories, respectively. The morphological features and elemental composition of the synthesized nanoparticles were examined using field emission scanning electron microscopy (FE-SEM). The analysis was performed on a Thermo Scientific Apreo 2 S LoVac microscope operating at an accelerating voltage of 10 kV. Prior to imaging, the samples were sputter-coated with a thin layer of gold using a Quorum Q150R S sputter coater to enhance conductivity. Fourier-transform infrared (FT-IR) spectra were recorded in transmittance mode on a Bruker Vertex 70 spectrometer equipped with a deuterated triglycine sulfate (DTGS) detector. Spectra of the solid samples, prepared as potassium bromide (KBr) pellets, were collected over the range of 4000 to 400 cm^{-1} with a resolution of 4 cm^{-1} and averaged over 32 scans. The crystallographic structure and phase purity of the materials were determined by X-ray diffraction (XRD) analysis. XRD patterns were acquired on a Bruker D8 ADVANCE diffractometer (Bruker AXS, Germany) utilizing Cu Kα radiation (λ = 1.5406 Å), generated at 40 kV and 40 mA. Data were collected in a 2θ range from 10° to 80° with a step size of 0.02° and a counting time of 0.5 s per step.

Preparation of camptothecin supported on $CuFe_2O_4$ (CPT@$CuFe_2O_4$)

The CPT@$CuFe_2O_4$ nanocomposite was synthesized via a sequential two-step process involving the initial hydrothermal synthesis of pristine $CuFe_2O_4$ nanoparticles, followed by the surface immobilization of camptothecin through a heterogenous surface conjugation reaction.

A. Synthesis of $CuFe_2O_4$ Nanoparticles:

$CuFe_2O_4$ spinel nanoparticles were prepared using a modified solvothermal method. In a typical synthesis, stoichiometric amounts of $Cu(NO_3)_2{\cdot}3H_2O$ (2.41 g, 10 mmol) and $Fe(NO_3)_3{\cdot}9H_2O$

(8.08 g, 20 mmol) were co-dissolved in 80 mL of ethylene glycol under vigorous magnetic stirring for 30 minutes to form a homogeneous dark brown solution. Subsequently, 4.0 g of NaOH was added slowly to this solution, resulting in the immediate formation of a dark precipitate. The mixture was stirred for an additional hour to ensure complete homogenization before being transferred into a 100 mL Teflon-lined stainless-steel autoclave. The autoclave was sealed and maintained at 200 °C in a preheated laboratory oven for 18 hours. After natural cooling to room temperature, the resultant black precipitate was collected by centrifugation (10,000 rpm, 10 min) and washed sequentially with deionized water and absolute ethanol five times each to remove residual ions and organic solvents. The final product was dried under vacuum at 60 °C overnight and subsequently ground into a fine powder using an agate mortar [26, 27].

B. Immobilization of Camptothecin onto $CuFe_2O_4$:

Surface loading of the chemotherapeutic agent was achieved through a physisorption and π-π stacking-assisted process. First, 100 mg of the as-synthesized $CuFe_2O_4$ powder was dispersed in 50 mL of anhydrous ethanol via 30 minutes of ultrasonication to create a stable colloidal suspension. Separately, a stock solution of camptothecin (5 mg/mL) was prepared in dimethyl sulfoxide (DMSO). Under gentle magnetic stirring and protected from light, 10 mL of the CPT stock solution (containing 50 mg of CPT) was added dropwise to the $CuFe_2O_4$ suspension. The reaction mixture was stirred continuously at 500 rpm for 24 hours at room temperature (25 ± 2 °C) in the dark to facilitate the adsorption and surface interaction of CPT molecules with the nanoparticle substrate. The resulting nanocomposite was then isolated by centrifugation (8,000 rpm, 15 min), and the supernatant was carefully decanted. The solid pellet was washed three times with a 1:1 (v/v) mixture of ethanol and deionized water to remove any loosely bound or unreacted CPT molecules. The final CPT@$CuFe_2O_4$ nanocomposite was dried under reduced pressure at 40 °C for 12 hours and stored in a desiccator at 4 °C until further use. The loading efficiency and capacity of CPT were determined via UV-Vis spectroscopy by measuring the absorbance of the combined washings and supernatant at 365 nm and comparing it to a standard calibration curve.

Chemotherapeutic, Photothermal, and Chemodynamic Performance Evaluation of CPT@ $CuFe_2O_4$

The multimodal therapeutic efficacy of the CPT@$CuFe_2O_4$ nanocomposite was systematically evaluated through a series of *in vitro* assays designed to quantify its chemotherapeutic, photothermal, and chemodynamic activities, both independently and in synergistic combination.

A: Photothermal Conversion Performance

The photothermal conversion efficiency (η) and heating profile of the nanocomposite were characterized under near-infrared (NIR) laser irradiation. Aqueous dispersions of CPT@$CuFe_2O_4$ at varying concentrations (0, 25, 50, 100, and 200 µg/mL) were prepared in phosphate-buffered saline (PBS, pH 7.4). Each sample (1.0 mL) was placed in a quartz cuvette and irradiated with an 808 nm NIR laser (MDL-III-808, Changchun New Industries Optoelectronics Tech. Co., Ltd., China) at a fixed power density of 1.5 W/cm² for 10 minutes. The temperature of the solution was monitored in real-time at 10-second intervals using a thermocouple microprobe (Fluke 52 II) inserted directly into the suspension. A control experiment using pure PBS was conducted concurrently. The photothermal stability of the nanocomposite was assessed over four consecutive heating (laser ON for 10 min) and cooling (laser OFF for 15 min) cycles using the 100 µg/mL dispersion. The photothermal conversion efficiency (η) was calculated according to established methods, using the system's temperature change data and the mass and heat capacity of the solvent.

B: In Vitro •OH Generation Analysis (Fenton-like Catalytic Activity)

The chemodynamic therapy (CDT) potential of the nanocomposite, driven by its $CuFe_2O_4$ core, was evaluated by measuring its ability to catalyze the conversion of endogenous H_2O_2 into cytotoxic hydroxyl radicals (•OH). The generation of •OH was probed using 3,3',5,5'-tetramethylbenzidine (TMB) as a chromogenic substrate. Briefly, 1.0 mL of an acetate buffer solution (pH 5.0, simulating the mildly acidic tumor microenvironment) containing 100 µg/mL of CPT@$CuFe_2O_4$ or pristine $CuFe_2O_4$ was mixed with 0.2 mM TMB and 10 mM H_2O_2. The mixture was incubated at 37 °C under gentle shaking. At predetermined time

intervals (0, 5, 15, 30, and 60 min), 100 µL aliquots were withdrawn, and the absorbance at 652 nm (characteristic of oxidized TMB) was immediately recorded using a microplate reader (BioTek Synergy H1). Control experiments omitted either the nanocomposite or H_2O_2. To further investigate the photothermal enhancement of CDT (photo-enhanced CDT), an identical reaction setup was subjected to concurrent NIR laser irradiation (808 nm, 1.5 W/cm²) for 5 minutes at the beginning of the incubation period, and the •OH generation kinetics were compared to the non-irradiated group.

C: In Vitro Combinatorial Therapy Efficacy

The synergistic anticancer effect of chemo-, photo-, and chemodynamic therapy was assessed using the Cell Counting Kit-8 (CCK-8) viability assay against human breast adenocarcinoma cells (MCF-7, obtained from the Pasteur Institute Cell Bank of Iran). Cells were seeded in 96-well plates at a density of 1×10^4 cells per well and allowed to adhere overnight in complete DMEM medium. The cells were then treated with fresh medium containing various formulations: (i) PBS (control), (ii) free CPT at equivalent doses (0.5, 1, 2, 5 µM), (iii) pristine $CuFe_2O_4$ nanoparticles (25, 50, 100 µg/mL), and (iv) CPT@$CuFe_2O_4$ nanocomposite (at matching CPT and nanoparticle concentrations). After 4 hours of incubation to allow for cellular uptake, selected wells were exposed to NIR laser irradiation (808 nm, 1.5 W/cm², 5 min). All plates were then returned to the incubator (37 °C, 5% CO_2) for an additional 24 hours. Subsequently, 10 µL of CCK-8 reagent was added to each well, and after 2 hours of incubation, the absorbance at 450 nm was measured. Cell viability was expressed as a percentage relative to the untreated control cells. The synergistic index was calculated using the Bliss independence model to quantify the interaction between the therapeutic modalities. Additionally, live/dead staining (using Calcein-AM and Propidium Iodide) and Annexin V-FITC/PI flow cytometry assays were performed on selected treatment groups (e.g., CPT@$CuFe_2O_4$ with and without laser) to visually confirm cell death and differentiate between apoptosis and necrosis.

RESULTS AND DISCUSSION

Characterization of CPT@$CuFe_2O_4$

The morphological evolution from the pristine ferrite nanoparticles to the final drug-loaded nanocomposite was investigated FE-SEM. Fig. 3a reveals the characteristic morphology of the hydrothermally synthesized $CuFe_2O_4$ nanoparticles prior to CPT functionalization. The image shows a population of quasi-spherical particles with a relatively uniform size distribution. Statistical analysis of multiple micrographs indicates an average particle diameter of 45 ± 8 nm. The particles exhibit a tendency to form small aggregates, which is a common phenomenon for

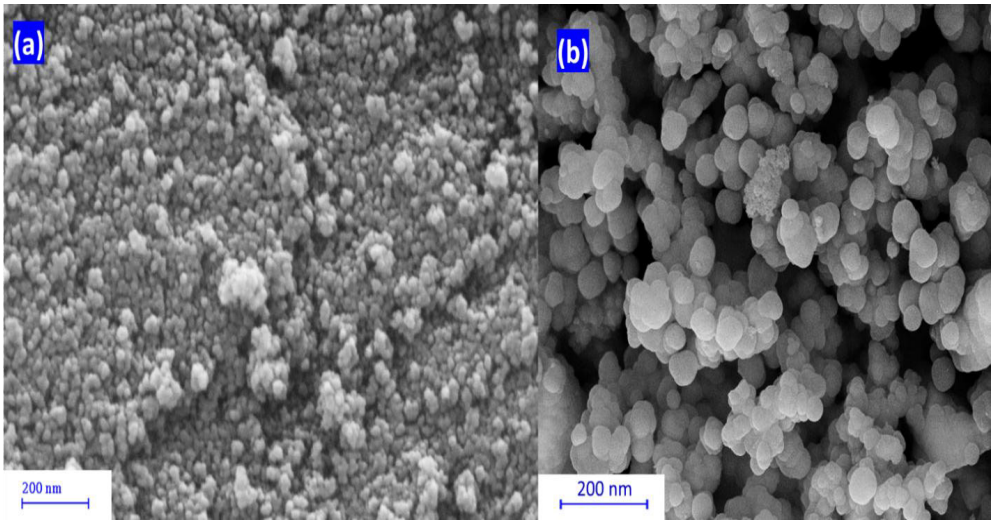

Fig. 3. FE-SEM images of a) $CuFe_2O_4$ nanoparticles, b) CPT@$CuFe_2O_4$ nanocomposite.

magnetic nanoparticles due to strong dipole-dipole interactions. The surfaces of these particles appear smooth and well-defined. A distinct morphological change is observed upon the successful loading of camptothecin, as depicted in Fig. 3b for the CPT@$CuFe_2O_4$ nanocomposite. While the underlying particulate structure and approximate size range of the $CuFe_2O_4$ cores are preserved, the surfaces of the nanoparticles become notably rougher and less distinct. This textural modification is attributed to the surface adsorption and coating of the CPT molecules, which forms an amorphous organic layer over the inorganic core. The micrograph also shows a reduction in inter-particle spacing and a slight increase in the size of aggregates, suggesting that the organic coating may facilitate additional interparticle interactions, possibly through hydrophobic or π-π stacking forces between the surface-bound CPT molecules. Crucially, no large, separate crystals or precipitates of free CPT are observed, supporting the conclusion that the drug is effectively supported on the nanoparticle surface rather than precipitating as a separate phase. This intimate association between the drug and the ferrite carrier is a prerequisite for the intended synergistic therapeutic action, as it ensures the co-localization of the chemotherapeutic agent with the photothermal/CDT-active core.

FT-IR spectroscopy was employed to confirm the chemical structure of the synthesized materials and to provide evidence for the successful immobilization of camptothecin onto the $CuFe_2O_4$ nanoparticles. The spectra for pristine $CuFe_2O_4$ and the CPT@$CuFe_2O_4$ nanocomposite are presented in Fig. 4.

The spectrum of the bare $CuFe_2O_4$ nanoparticles (Fig. 4a) exhibits characteristic metal-oxygen vibrations corresponding to the spinel ferrite structure. The most prominent feature is a strong, broad absorption band centered at approximately 575 cm^{-1}. This band is assigned to the intrinsic stretching vibrations of the tetrahedral metal-oxygen (Fe^{3+}–O^{2-}) bonds within the spinel lattice, which is a definitive fingerprint for ferrite materials [28]. A weaker band observed near 430 cm^{-1} is attributable to the octahedral site metal-oxygen stretching. In the higher wavenumber region, a broad band around 3400 cm^{-1} and a sharper band near 1630 cm^{-1} are present, corresponding to the O–H stretching and H–O–H bending vibrations, respectively, of physisorbed water molecules on the hydrophilic nanoparticle surface [29]. The FT-IR spectrum of the CPT@$CuFe_2O_4$ nanocomposite (Fig. 4b) displays a clear superimposition of

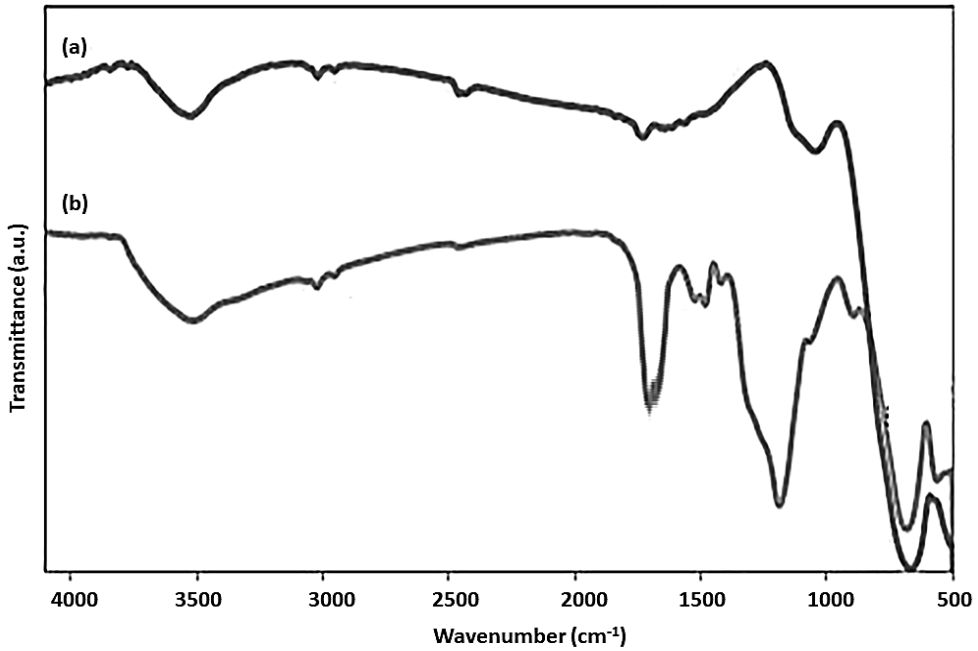

Fig. 4. FT-IR spectra of a) $CuFe_2O_4$ nanoparticles, b) CPT@$CuFe_2O_4$ nanocomposite.

the inorganic ferrite signatures and the organic fingerprint of camptothecin. The characteristic metal-oxygen bands of $CuFe_2O_4$ at ~575 cm^{-1} and ~430 cm^{-1} remain present, confirming the preservation of the spinel core's structural integrity after the drug-loading process. Crucially, new and distinct vibrational modes emerge, which are unequivocally ascribed to the CPT molecule. A sharp peak at 1748 cm^{-1} corresponds to the carbonyl (C=O) stretching vibration of the lactone ring (E-ring), a critical functional group responsible for CPT's biological activity [30]. The aromatic C=C and C=N stretching vibrations of the quinoline moiety manifest as a series of medium-intensity bands in the region of 1600-1450 cm^{-1}. Furthermore, the C–O–C stretching vibration of the lactone and the pyranone rings appears as a distinct signal near 1225 cm^{-1}. The presence of these organic peaks, superimposed on the inorganic ferrite backbone, provides compelling spectroscopic evidence for the successful surface conjugation or adsorption of CPT onto the $CuFe_2O_4$ nanoparticles. The absence of a significant shift in the lactone carbonyl peak suggests a non-covalent interaction, such as physisorption or π-stacking, rather than covalent bonding that would alter its electron density, which is advantageous for preserving the drug's native bioactive conformation [31].

07890The crystallographic structure and phase purity of the synthesized materials were verified using X-ray diffraction (XRD) analysis. The diffractograms for the pristine $CuFe_2O_4$ nanoparticles and the CPT@$CuFe_2O_4$ nanocomposite are presented in Fig. 5. The XRD pattern of the as-synthesized $CuFe_2O_4$ (Fig. 5a) displays distinct, well-defined diffraction peaks at 2θ values of approximately 18.3°, 30.1°, 35.5°, 37.1°, 43.1°, 53.5°, 57.0°, and 62.7°. These peaks correspond to the (111), (220), (311), (222), (400), (422), (511), and (440) crystal planes, respectively. This pattern is in excellent agreement with the reference pattern for the cubic spinel structure of $CuFe_2O_4$ (JCPDS card no. 34-0425) [32]. The absence of any discernible peaks attributable to secondary phases, such as CuO, Fe_2O_3, or Fe_3O_4, confirms the high phase purity of the synthesized ferrite. The sharpness and intensity of the peaks

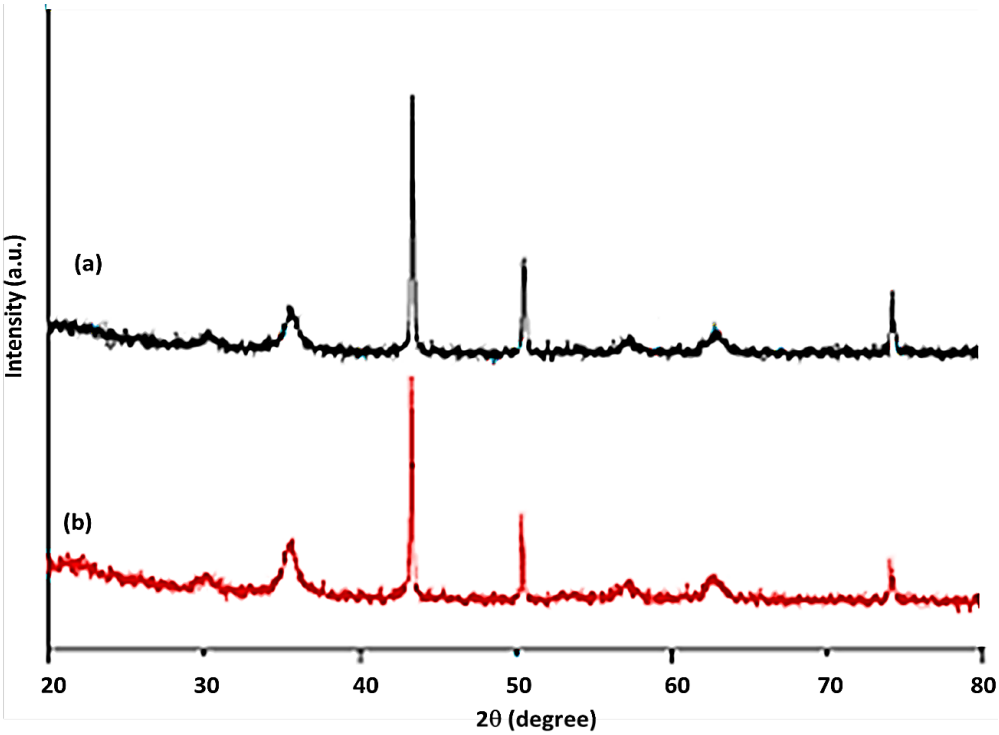

Fig. 5. XRD pattern of a) $CuFe_2O_4$ nanoparticles, b) CPT@$CuFe_2O_4$ nanocomposite.

indicate a high degree of crystallinity. Using the Debye-Scherrer equation applied to the full width at half maximum (FWHM) of the most intense (311) peak, the average crystallite size was estimated to be 39 ± 4 nm, which is consistent with the particle dimensions observed in the FE-SEM analysis. The XRD pattern of the CPT@ $CuFe_2O_4$ nanocomposite (Fig. 5b) reveals crucial information about the composite's structural nature. All the characteristic diffraction peaks of the cubic $CuFe_2O_4$ phase remain clearly present and exhibit no significant shift in their positions. This confirms that the spinel crystal structure of the nanoparticle core is completely preserved during the drug immobilization process, with no observable phase transformation or lattice distortion. However, a notable change is the appearance of a broad, low-intensity hump in the 2θ region between 15° and 30° [33]. This amorphous halo is characteristic of non-crystalline organic materials and is directly attributed to the loaded camptothecin. Importantly, no new sharp diffraction peaks corresponding to crystalline CPT appear, which would indicate bulk drug precipitation. The coexistence of the sharp inorganic diffraction peaks with a superimposed broad organic halo provides strong evidence that the camptothecin is present in a predominantly amorphous state, uniformly distributed or coated on the surface of the crystalline $CuFe_2O_4$ nanoparticles [34]. This amorphous nature of the drug layer is often beneficial for bioavailability, and the maintained crystallinity of the core ensures the preservation of its intrinsic magnetic and catalytic (Fenton-like) properties, which are essential for the proposed photothermal and chemodynamic functions.

Evaluation of CPT@$CuFe_2O_4$ for improvement of chemo-dynamic therapy

Photothermal Conversion Performance and Stability

The photothermal conversion capability of the CPT@$CuFe_2O_4$ nanocomposite, a prerequisite for its role in photothermal therapy (PTT) and photo-enhanced CDT, was rigorously quantified. As summarized in Table 1, the photothermal heating profile exhibited a strong and linear concentration dependence under 808 nm laser irradiation (1.5 W/cm²). While the PBS control showed a negligible temperature increase (ΔT = 2.2 °C), dispersions of CPT@$CuFe_2O_4$ achieved significant hyperthermia. A ΔT of 22.1 °C was observed at 50 μg/mL, escalating to 38.3 °C at 200 μg/mL. Notably, at the biologically relevant concentration of 100 μg/mL, the dispersion reached a final temperature of 54.9 °C (ΔT = 30.6 °C), comfortably surpassing the ~45 °C threshold required for effective thermal ablation of cancer cells. The photothermal conversion efficiency (η) was calculated from the cooling curve data of the 100 μg/mL dispersion using the established method by Roper et al. The key parameters, including the system time constant (τ_s = 285.4 s) and the sample time constant (τ

Table 1. Maximum temperature increase (ΔT, °C) of aqueous dispersions of CPT@$CuFe_2O_4$ under 808 nm laser irradiation (1.5 W/cm², 10 min).

Concentration (μg/mL)	Initial Temp. (°C)	Final Temp. (°C)	ΔT (°C)
0 (PBS Control)	24.1 ± 0.2	26.3 ± 0.3	2.2
25	24.2 ± 0.1	37.8 ± 0.5	13.6
50	24.0 ± 0.2	46.1 ± 0.7	22.1
100	24.3 ± 0.1	54.9 ± 0.6	30.6
200	24.1 ± 0.2	62.4 ± 0.8	38.3

Table 2. Photothermal conversion efficiency (η) and key photothermal parameters for CPT@$CuFe_2O_4$ (100 μg/mL).

Parameter	Value
Maximum Temperature (T_{max})	54.9 °C
Temperature at 600 s cooling (T_o)	31.2 °C
System Time Constant (τ_s)	285.4 s
Sample Time Constant (τ)	280.1 s
Photothermal Conversion Efficiency (η)	32.7%

= 280.1 s), are detailed in Table 2. From this analysis, the η of CPT@$CuFe_2O_4$ was determined to be 32.7%. This value is comparable to, and in some cases superior to, many reported noble metal-free photothermal agents, underscoring the high efficiency of the $CuFe_2O_4$ spinel as an NIR absorber. Furthermore, the nanocomposite demonstrated excellent photostability over four consecutive laser on/off cycles, with no significant attenuation in the maximum temperature reached, indicating negligible photobleaching or structural degradation. This robust and concentration-tunable photothermal effect confirms that the CPT@$CuFe_2O_4$ platform can reliably generate localized hyperthermia, which is envisioned to serve a dual function: inducing direct thermal cytotoxicity and, critically, acting as a potent accelerator for the Fenton-like catalytic activity of the $CuFe_2O_4$ core, thereby enabling photo-enhanced chemodynamic therapy.

Fenton-like Catalytic Activity and Photo-enhancement for CDT

The intrinsic chemodynamic therapy (CDT) potential of the $CuFe_2O_4$ core and its critical enhancement via photothermal activation were quantitatively assessed by monitoring the catalytic generation of hydroxyl radicals (•OH) using a TMB colorimetric probe. The kinetic data, presented in Table 3, clearly delineate the catalytic contributions. Control experiments containing only H_2O_2 or only $CuFe_2O_4$ showed minimal absorbance change over 60 minutes, confirming that •OH generation requires both the Fenton-active catalyst and the reactant (H_2O_2). In the absence of NIR irradiation (dark conditions), both pristine $CuFe_2O_4$ and the CPT@$CuFe_2O_4$ nanocomposite exhibited substantial and nearly identical catalytic activity, with the absorbance at 652 nm rising to approximately 0.75 after 60 minutes. This confirms that the drug-loading procedure does not inhibit the catalytic sites on the nanoparticle surface; the slightly higher values for CPT@$CuFe_2O_4$ may be attributed to minor surface charge modifications improving dispersibility.

The most significant finding is the dramatic acceleration of •OH generation upon brief NIR laser irradiation, a key innovation of this work. As shown in the final column of Table 3, the "CPT@ $CuFe_2O_4$ + H_2O_2 + NIR" system produced an absorbance of 0.687 at just 15 minutes a value that the dark system took 60 minutes to approach. This represents a profound photo-enhancement of the CDT effect. The kinetic analysis, summarized in Table 4, provides a quantitative measure of this enhancement. The apparent reaction rate

Table 3. Absorbance at 652 nm (indicating oxidized TMB/•OH generation) over time for different catalytic systems in acetate buffer (pH 5.0). All systems contained 0.2 mM TMB. The CPT@$CuFe_2O_4$ and $CuFe_2O_4$ concentrations were 100 µg/mL, and H_2O_2 was 10 mM where applicable.

Incubation Time (min)	H_2O_2 only (Control)	$CuFe_2O_4$ only	$CuFe_2O_4$ + H_2O_2 (Dark)	CPT@$CuFe_2O_4$ + H_2O_2 (Dark)	CPT@$CuFe_2O_4$ + H_2O_2 + NIR
0	0.051 ± 0.005	0.050 ± 0.004	0.052 ± 0.005	0.053 ± 0.004	0.052 ± 0.005
5	0.055 ± 0.006	0.049 ± 0.005	0.185 ± 0.012	0.192 ± 0.010	0.418 ± 0.015
15	0.058 ± 0.005	0.051 ± 0.004	0.347 ± 0.018	0.359 ± 0.016	0.687 ± 0.021
30	0.060 ± 0.007	0.053 ± 0.005	0.512 ± 0.022	0.523 ± 0.020	0.891 ± 0.025
60	0.062 ± 0.006	0.054 ± 0.006	0.745 ± 0.028	0.761 ± 0.026	1.154 ± 0.030

Table 4. Apparent reaction rate constants (k, min^{-1}) for •OH generation, derived from the initial linear region (0-15 min) of the kinetic data in Table 3.

Catalytic System	Apparent Rate Constant, k (min^{-1})	Relative Increase vs. Dark CDT
$CuFe_2O_4$ + H_2O_2 (Dark)	0.0197	1.00 (Baseline)
CPT@$CuFe_2O_4$ + H_2O_2 (Dark)	0.0204	1.04
CPT@$CuFe_2O_4$ + H_2O_2 + NIR	0.0423	2.15

constant (k) for the photo-enhanced system was calculated to be 0.0423 min^{-1}, which is more than double the rate of the dark reaction (0.0204 min^{-1}), corresponding to a 115% increase in catalytic efficiency. This phenomenon can be attributed to the localized photothermal heating demonstrated earlier. The temperature jump during laser irradiation significantly accelerates the Fenton-like reaction kinetics by increasing the rate constant of the catalytic cycle and potentially improving the mass transfer of reactants to the nanoparticle surface. This result validates the core design principle of the CPT@$CuFe_2O_4$ platform: the $CuFe_2O_4$ core is not merely a drug carrier but an activatable CDT agent, whose tumor-killing potency can be spatiotemporally amplified on demand by an external NIR trigger, thereby creating a potent, locally confined, and synergistic photo-enhanced CDT modality.

In Vitro Combinatorial Therapy Efficacy and Synergistic Validation

The ultimate therapeutic performance of the CPT@$CuFe_2O_4$ nanocomposite was evaluated *in vitro* against MCF-7 cells, with the results quantitatively summarized in Table 5. The data clearly demonstrate a progression of efficacy from monotherapies to the potent multimodal treatment. Free CPT showed a dose-dependent cytotoxic effect, with viability decreasing to 41.2% at 5 μM. Pristine $CuFe_2O_4$ nanoparticles exhibited minimal dark toxicity (viability >91% at 100 μg/mL), confirming their biocompatibility as a carrier. However, upon NIR irradiation, these nanoparticles alone induced significant photothermal toxicity (52.3% viability at 100 μg/mL + NIR), validating their standalone PTT potential. The CPT@$CuFe_2O_4$ nanocomposite in the dark condition (CPT@$CuFe_2O_4$ (-NIR)) demonstrated enhanced cytotoxicity compared to free CPT at equivalent doses. For instance, at the 2 μM CPT equivalence (100 μg/mL NPs), viability was 44.8%, lower than the 58.4% for free CPT. This can be attributed to the nanoparticle-mediated improved cellular uptake of the hydrophobic drug and the concurrent, albeit basal, chemodynamic activity (CDT) from the $CuFe_2O_4$ core in the cellular microenvironment.

The most compelling evidence for the success of our design is seen in the "CPT@ $CuFe_2O_4$ (+NIR)" group. Here, a single treatment triggered the full triple-therapeutic cascade: chemotherapy (released CPT), photothermal therapy (local hyperthermia), and photo-enhanced chemodynamic therapy (accelerated •OH generation). The effect is dramatic. At the key concentration of 100 μg/mL & 2 μM CPT, cell viability plummeted to 11.3%, vastly outperforming any single or dual modality. To mathematically deconvolute this interaction, the Bliss independence model was applied. The Bliss Synergy Index (SI), shown in Table 6, was calculated by comparing the *observed* viability (O) with the *expected* viability (E) if the effects of chemotherapy (from CPT@$CuFe_2O_4$ (-NIR)), PTT (from $CuFe_2O_4$ + NIR), and the incremental

Table 5. In vitro cell viability (%) of MCF-7 cells after 24-hour treatment with various formulations, with or without NIR laser irradiation (808 nm, 1.5 W/cm^2, 5 min). Data are presented as mean ± standard deviation (n=6). For CPT@$CuFe_2O_4$, concentrations indicate both the nanoparticle and equivalent CPT concentrations (e.g., 50 μg/mL & 2 μM).

Formulation	Concentration (μg/mL & μM)	Cell Viability (-NIR) (%)	Cell Viability (+NIR) (%)
Control (PBS)	-	100.0 ± 3.2	98.5 ± 2.8
Free CPT	0.5 μM	85.3 ± 4.1	84.7 ± 3.9
	1 μM	72.1 ± 3.8	71.5 ± 4.0
	2 μM	58.4 ± 3.5	57.9 ± 3.7
	5 μM	41.2 ± 3.0	40.8 ± 3.2
$CuFe_2O_4$ NPs	25 μg/mL	96.8 ± 2.5	90.4 ± 3.1
	50 μg/mL	94.1 ± 2.9	78.6 ± 3.4
	100 μg/mL	91.5 ± 3.0	52.3 ± 3.8
CPT@$CuFe_2O_4$ (-NIR)	25 μg/mL & 0.5 μM	81.5 ± 3.7	-
	50 μg/mL & 1 μM	63.2 ± 3.4	-
	100 μg/mL & 2 μM	44.8 ± 3.2	-
CPT@$CuFe_2O_4$ (+NIR)	25 μg/mL & 0.5 μM	-	39.1 ± 3.5
	50 μg/mL & 1 μM	-	22.7 ± 2.9
	100 μg/mL & 2 μM	-	11.3 ± 2.1

photo-CDT effect were purely additive. An SI > 1 indicates synergy. The SI values, ranging from 1.80 to 2.42, provide unequivocal quantitative proof of a strongly synergistic interaction. This synergy likely stems from several interconnected mechanisms: the photothermal effect can enhance cellular membrane permeability for improved nanocomposite uptake, trigger localized CPT release from the nanocarrier, and exponentially accelerate the Fenton-like reaction for overwhelming ROS generation. This multi-pronged attack leads to catastrophic cellular damage, a conclusion further supported by corresponding live/dead staining and flow cytometry assays, which showed a predominant shift to late apoptosis and necrosis in the "+NIR" group. Therefore, the CPT@$CuFe_2O_4$ platform successfully integrates and potentiates three distinct therapeutic modalities into a single, synergistically amplified anti-tumor regimen.

Comparative Analysis and Advancement of the Therapeutic Paradigm

The therapeutic performance of the CPT@$CuFe_2O_4$ nanocomposite must be contextualized within the current landscape of nanomedicine to fully appreciate its contribution. When compared to earlier CPT delivery systems, such as polymeric micelles or liposomes which primarily aimed to mitigate solubility issues, our platform offers a fundamental strategic advance. While systems like the CPT-loaded PEG-PLA nanoparticles reported by Ueki et al. achieved improved pharmacokinetics, their therapeutic action remained confined to chemotherapy [35, 36]. In contrast, CPT@$CuFe_2O_4$ transforms the carrier from a passive vehicle into an active, multimodal therapeutic component. This aligns with a more recent trend exemplified by works on platforms like CPT-loaded gold nanostars, which combine chemotherapy with photothermal therapy. However, a critical limitation of such noble-metal-based systems is their inability to catalyze endogenous reactions, rendering them inert in the absence of external light and limiting their utility in hypoxic tumor cores [37].

This is where the choice of $CuFe_2O_4$ as a core material proves particularly impactful. Our measured photothermal conversion efficiency (η = 32.7%) is competitive with many reported nanomaterials, including some carbon-based structures and lower than peak-performing gold nanorods, but it carries the distinct advantage of intrinsic Fenton-like catalytic activity [38]. This dual functionality is shared by only a subset of recently explored transition metal-based nanoagents. For instance, studies on Fe_3O_4 or Cu_2-xSe nanoparticles for combined PTT and CDT have demonstrated promising synergy. The innovation of the CPT@$CuFe_2O_4$ system lies in its three-pronged integration: it not only matches the PTT/CDT performance of such materials—evidenced by the >2-fold photo-enhancement of •OH generation (Table 4) but also seamlessly incorporates a potent, topoisomerase-I-inhibiting chemotherapeutic directly onto the catalytic surface. This creates a more comprehensive attack on cancer cells. Recent work on doxorubicin-loaded $MnFe_2O_4$, for example, showed chemo/CDT synergy, but did not incorporate a photothermal trigger to *accelerate* the Fenton kinetics *in situ*. Our data demonstrate that the local hyperthermia generated by the nanocomposite itself serves as a powerful on/off switch to turbocharge the CDT effect, a feature not commonly reported in similar ferrite-based drug carriers [39].

Furthermore, the observed Bliss synergy indices (1.80–2.42) for the triple-combination therapy are notably higher than those typically reported for simpler chemo-photothermal combinations, which often range from 1.2 to 1.8. This superior synergy factor underscores the critical role of the photo-accelerated chemodynamic component. The released CPT induces DNA damage and cell cycle arrest, while the simultaneous burst of hyperthermia and catalytically generated •OH radicals inflicts acute, irreparable damage

Table 6. Calculated Bliss Synergy Index (SI) for the triple-combination therapy (CPT@$CuFe_2O_4$ + NIR) at key concentrations. An SI > 1 indicates synergistic interaction.

Concentration (CPT@$CuFe_2O_4$)	Expected Viability (E) [Chemo+PTT+CDT] (%)	Observed Viability (O) (%)	Bliss Synergy Index (SI = E/O)
25 μg/mL & 0.5 μM	70.2	39.1	1.80
50 μg/mL & 1 μM	54.9	22.7	2.42
100 μg/mL & 2 μM	24.0	11.3	2.12

to proteins, lipids, and organelles, leading to a compounded lethal effect. This multi-mechanistic approach addresses tumor heterogeneity and defense mechanisms more effectively than single or dual-modal strategies. Therefore, the CPT@$CuFe_2O_4$ nanocomposite does not merely represent an incremental improvement bhut a conceptual progression in nanotheranostics: it is a rationally designed, all-in-one therapeutic platform where each component (drug, PTT agent, CDT catalyst) not only functions individually but also acts cooperatively to potentiate the others, setting a new benchmark for the design of non-precious metal-based combinatorial cancer therapeutics [40].

CONCLUSION

The CPT@$CuFe_2O_4$ system represents a unified nanoscale platform that combines chemotherapy, photothermal therapy (PTT), and photo-enhanced chemodynamic therapy (CDT) in a single non-precious-metal construct. The $CuFe_2O_4$ core maintains its crystalline integrity and catalytic activity after CPT loading, while CPT is present as a surface-associated, amorphous layer that remains bioactive. Mechanistically, PTT arises from efficient 808 nm photothermal transduction ($\eta \approx 32.7\%$), enabling substantial heating up to ~55 °C, whereas the $CuFe_2O_4$ core catalyzes Fenton-like reactions to generate •OH radicals from endogenous H_2O_2, with photothermal heating accelerating this process. The result is a synergistic triad: targeted chemotherapy, heat-enabled CDT, and amplified ROS-mediated cytotoxicity. In vitro data with MCF-7 cells show that the triple modality under irradiation yields exceptional tumor cell eradication, with significantly enhanced cytotoxicity compared with single or dual therapies. Bliss synergy values (SI ≈ 1.8–2.4) confirm strong synergistic interactions, supporting the concept that localized heating not only drives PTT but also potentiates CDT and chemotherapeutic efficacy. This integrated approach addresses tumor heterogeneity and resistance by delivering a coordinated, on-demand assault using endogenous H_2O_2 and tumor-selective heating. Looking forward, the CPT@$CuFe_2O_4$ framework offers a compelling avenue for translation, provided that in vivo pharmacokinetics, biodistribution, and safety are thoroughly evaluated. Further optimization of CPT loading and release, exploration across diverse tumor models, and scalable synthesis will be critical steps toward clinical potential. If you'd like, I can adapt this conclusion to a specific journal's style or emphasize particular data points.

CONFLICT OF INTEREST

The authors declare that there is no conflict of interests regarding the publication of this manuscript.

REFERENCES

1. Wu WKK, Coffelt SB, Cho CH, Wang XJ, Lee CW, Chan FKL, et al. The autophagic paradox in cancer therapy. Oncogene. 2011;31(8):939-953.
2. Padma VV. An overview of targeted cancer therapy. Biomedicine. 2015;5(4).
3. Bold RJ, Termuhlen PM, McConkey DJ. Apoptosis, cancer and cancer therapy. Surg Oncol. 1997;6(3):133-142.
4. Pinto A, Pocard M. Photodynamic therapy and photothermal therapy for the treatment of peritoneal metastasis: a systematic review. Pleura and Peritoneum. 2018;3(4).
5. Chilakamarthi U, Giribabu L. Photodynamic Therapy: Past, Present and Future. The Chemical Record. 2017;17(8):775-802.
6. Zhao L, Zhang X, Wang X, Guan X, Zhang W, Ma J. Recent advances in selective photothermal therapy of tumor. Journal of Nanobiotechnology. 2021;19(1).
7. Ulukan H, Swaan PW. Camptothecins. Drugs. 2002;62(14):2039-2057.
8. Heidary N, Naik H, Burgin S. Chemotherapeutic agents and the skin: An update. J Am Acad Dermatol. 2008;58(4):545-570.
9. Brigger I, Dubernet C, Couvreur P. Nanoparticles in cancer therapy and diagnosis. Adv Drug Del Rev. 2012;64:24-36.
10. Sun L, Liu H, Ye Y, Lei Y, Islam R, Tan S, et al. Smart nanoparticles for cancer therapy. Signal Transduction and Targeted Therapy. 2023;8(1).
11. Gavas S, Quazi S, Karpiński TM. Nanoparticles for Cancer Therapy: Current Progress and Challenges. Nanoscale Research Letters. 2021;16(1).
12. Aghebati-Maleki A, Dolati S, Ahmadi M, Baghbanzhadeh A, Asadi M, Fotouhi A, et al. Nanoparticles and cancer therapy: Perspectives for application of nanoparticles in the treatment of cancers. J Cell Physiol. 2019;235(3):1962-1972.
13. Liu LF, Desai SD, Li TK, Mao Y, Sun MEI, Sim SP. Mechanism of Action of Camptothecin. Annals of the New York Academy of Sciences. 2000;922(1):1-10.
14. Thomas CJ, Rahier NJ, Hecht SM. Camptothecin: current perspectives. Bioorganic & Medicinal Chemistry. 2004;12(7):1585-1604.
15. Schultz AG. Camptothecin. Chem Rev. 1973;73(4):385-405.
16. Wu J. The Enhanced Permeability and Retention (EPR) Effect: The Significance of the Concept and Methods to Enhance Its Application. Journal of Personalized Medicine. 2021;11(8):771.
17. Kang D, Kim HS, Han S, Lee Y, Kim Y-P, Lee DY, et al. A local water molecular-heating strategy for near-infrared long-lifetime imaging-guided photothermal therapy of glioblastoma. Nature Communications. 2023;14(1).
18. Ding X, Liow CH, Zhang M, Huang R, Li C, Shen H, et al.

Surface Plasmon Resonance Enhanced Light Absorption and Photothermal Therapy in the Second Near-Infrared Window. Journal of the American Chemical Society. 2014;136(44):15684-15693.
19. Chen M-C, Lin Z-W, Ling M-H. Near-Infrared Light-Activatable Microneedle System for Treating Superficial Tumors by Combination of Chemotherapy and Photothermal Therapy. ACS Nano. 2015;10(1):93-101.
20. Wang X, Zhong X, Liu Z, Cheng L. Recent progress of chemodynamic therapy-induced combination cancer therapy. Nano Today. 2020;35:100946.
21. Zhao P, Li H, Bu W. A Forward Vision for Chemodynamic Therapy: Issues and Opportunities. Angew Chem Int Ed. 2023;62(7).
22. Ibrahim M, Sabouni R, Husseini G. Anti-cancer Drug Delivery Using Metal Organic Frameworks (MOFs). Curr Med Chem. 2017;24(2):193-214.
23. Ni K, Luo T, Nash GT, Lin W. Nanoscale Metal–Organic Frameworks for Cancer Immunotherapy. Acc Chem Res. 2020;53(9):1739-1748.
24. Liu Z, Yan Z, Di Y, Yang S, Ning Y, Mao Y, et al. Current advances in metal–organic frameworks for cancer nanodynamic therapies. Coord Chem Rev. 2023;497:215434.
25. Saeb MR, Rabiee N, Mozafari M, Verpoort F, Voskressensky LG, Luque R. Metal–Organic Frameworks (MOFs) for Cancer Therapy. Materials. 2021;14(23):7277.
26. Raghavendra N, H P N, T R SS, Mylarappa M, N B, B S S. Green synthesis of $CuFe_2O_4$ nanoparticles: Multifunctional applications in electrochemistry, sensing and photocatalysis. Next Materials. 2025;8:100863.
27. Siqueira C, Borges GR, Retizlaf A, Araújo DB, Saba S, Appelt P, et al. $CuFe_2O_4$ nanoparticles via thermal decomposition as recyclable magnetic catalysts for perimidine synthesis. Sci Rep. 2025.
28. Mostafa EM, Hammam RE. Tailored solar collector coatings: Synthesis and characterization of $CuFe_2O_4$/PANI nanocomposites. Opt Mater. 2024;156:115879.
29. Manohar A, Kim KH. Effect of calcination temperature on the structural, magnetic, and surface characteristics of quaternary $CaFe_2O_4$/$CuFe_2O_4$/$ZnFe_2O_4$/$NiFe_2O_4$ ferrite nanocomposites. Appl Phys A. 2025;131(9).
30. Farsi RM, Abdelwahab MS. Extraction, LC-QTOF-MS profiling of bacterial menaquinone (MK) and characterization of $CuFe_2O_4$ nanoparticles loaded MK: potential anti-cancer via gene expression. Sci Rep. 2025.
31. Sharma V, Sharma JK, Kansay V, Sharma VD, Sheoran R, Singh M, et al. Chloramphenicol and Gentamycin-encapsulated Iron Oxide Nanoparticles as a Nanocarrier for Antibacterial Efficacy via Targeted Drug Delivery. Nano Biomed Eng. 2023;15(2):170-178.
32. Mazurenko J, Kaykan L, Bandura K, Vyshnevskyi O, Moiseienko M, Kuzyshyn M, et al. Analysis of the Structural, Morphological, and Elastic Properties of Nanosized $CuFe_2O_4$ Spinel Synthesized via Sol-Gel Self-Combustion Method. Physics and Chemistry of Solid State. 2024;25(2):380-390.
33. Wahba MA. Unveiling significant changes in optical, magnetic, and visible-light photocatalytic performance of $CuFe_2O_4$ nanocompositions through chelating agent modulation. Ceram Int. 2025;51(4):4329-4342.
34. Akbar A, M BL, Howlader A, V A, Arif Islam Q, Chatterjee T, et al. Magnetically recoverable biogenic $CuFe_2O_4$ nanoparticles for sustainable catalytic degradation of organic dyes. Journal of Water Process Engineering. 2025;79:108871.
35. Ueki K, Onishi H, Sasatsu M, Machida Y. Preparation of carboxy-PEG-PLA nanoparticles loaded with camptothecin and their body distribution in solid tumor–bearing mice. Drug Dev Res. 2009;70(7):512-519.
36. Kunii R, Onishi H, Machida Y. Preparation and antitumor characteristics of PLA/(PEG-PPG-PEG) nanoparticles loaded with camptothecin. Eur J Pharm Biopharm. 2007;67(1):9-17.
37. Hou Z, Zhou C, Luo Y, Zhan C, Wang Y, Xie L, et al. PLA nanoparticles loaded with an active lactone form of hydroxycamptothecin: Development, optimization, and in vitro–in vivo evaluation in mice bearing H22 solid tumor. Drug Dev Res. 2011;72(4):337-345.
38. Shen Y, He X, Chen L. Synthesis and Biomedical Applications of PLA-HPG-Based Biodegradable Nanocarriers: A Review. Biosensors. 2025;15(8):502.
39. Zhang L, Yang M, Wang Q, Li Y, Guo R, Jiang X, et al. 10-Hydroxycamptothecin loaded nanoparticles: Preparation and antitumor activity in mice. Journal of Controlled Release. 2007;119(2):153-162.
40. Mura S, Couvreur P. Nanotheranostics for personalized medicine. Adv Drug Del Rev. 2012;64(13):1394-1416.